JACS
JOURNAL OF THE AMERICAN CHEMICAL SOCIETY
Article
pubs.acs.org/JACS

Differential Role of the Protein Matrix on the Binding of a Catalytic Aspartate to Mg^{2+} vs Ca^{2+}: Application to Ribonuclease H

C. Satheesan Babu,*[,†] Todor Dudev,[†] and Carmay Lim*[,†,‡]

[†]Institute of Biomedical Sciences, Academia Sinica, Taipei 11529, Taiwan
[‡]Department of Chemistry, National Tsing Hua University, Hsinchu 300, Taiwan

Supporting Information

ABSTRACT: Divalent metal cations are essential cofactors for many enzyme functions. Although Mg^{2+} is the native cofactor in many enzymes such as ribonuclease H, its competitor Ca^{2+} may also bind to the enzyme but inhibit catalysis. Thus, the competition between Mg^{2+} and Ca^{2+} for a given metal-binding site in an enzyme and their effects on enzyme activity are of great interest. Most studies have focused on the interactions between Mg^{2+} or Ca^{2+} and the metal ligands in the first and sometimes second coordination shell. However, no study (to our knowledge) has examined the role of the protein architecture and surrounding aqueous environment on the binding of Mg^{2+} vs Ca^{2+} to a given protein metal-binding site. In this work, the free energy barriers for the binding of a catalytically essential aspartate to Mg^{2+} or Ca^{2+} in ribonuclease H from two organisms were computed using umbrella sampling with a classical force field ("classical" model). The corresponding free energy barriers in water were computed using the "classical" model as well as density functional theory combined with a self-consistent reaction field. The results reveal that, relative to water, the protein architecture and coupled protein−water interactions raise the free energy barrier for binding of the catalytically essential aspartate to the native Mg^{2+} cofactor more than the respective binding to Ca^{2+}. They also reveal the physical basis for the different observed binding modes of Mg^{2+} and Ca^{2+} and highlight limitations of simulations with classical force fields that do not explicitly account for charge transfer and polarization effects.

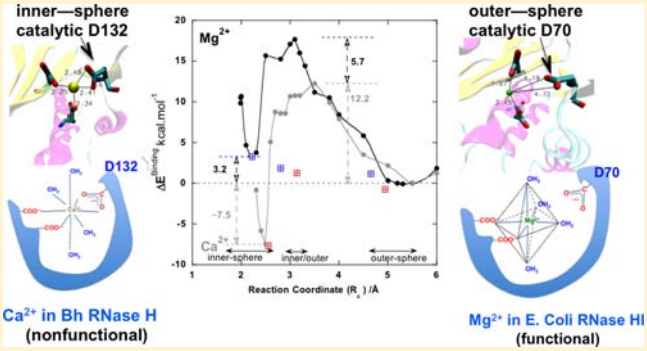

INTRODUCTION

Divalent metal cations are essential for the function of many proteins whose metal-dependent functions include enzyme catalysis, signal transduction, respiration, and photosynthesis.[1−5] Among a pool of biogenic divalent cations such as Mg^{2+}, Ca^{2+}, Mn^{2+}, Fe^{2+}, Co^{2+}, Ni^{2+}, Cu^{2+}, and Zn^{2+}, most nucleases, especially endoribonucleases, selectively bind to Mg^{2+} or Mn^{2+} for enzymatic activity.[3,6] The metal-binding site in these enzymes is usually composed of a triad of conserved Asp/Glu residues. However, the native Mg^{2+} (or Mn^{2+}) cofactor faces stiff competition from Ca^{2+}, which could also bind to the enzyme but inhibit catalysis.[7] Indeed, Ca^{2+} is found to bind to *Escherichia coli* ribonuclease HI (*E. coli* RNase HI) in solution tighter than the native Mg^{2+} cofactor, but it abolishes enzymatic activity.[8−10] Thus, the competition between Mg^{2+} and Ca^{2+} for a given metal-binding site in an enzyme and their effect on enzyme activity are of great interest.

We focus on the enzyme ribonuclease H (RNase H), a member of the nucleotidyl-transferase superfamily. RNase H is a sequence-nonspecific, Mg^{2+} (or Mn^{2+})-dependent endonuclease that specifically cleaves the RNA strand of DNA·RNA hybrids.[11,12] We chose to study this enzyme because 3D structures of RNase H from different organisms bound to Ca^{2+} and/or Mg^{2+} have been solved and the free energies of alkaline earth (group IIA) metal dications binding to *E. coli* RNase HI have been measured.[10,13] RNase H enzymes possess a DED′ metal-binding motif comprising three conserved carboxylates. The first two carboxylates (D and E) are bound monodentately to the metal ion in the RNase H structures, but the third carboxylate (D′) is seen at different distances and orientations relative to the metal ion (see Figure 1). D′ is a catalytically essential residue, as its mutation in *E. coli* RNase HI to Asn inactivates the enzyme even when Mg^{2+} is present.[14] In the Mg^{2+}-bound X-ray structure of *E. coli* RNase HI (Figure 1a),[15] D′ (D70) is >4 Å from Mg^{2+}, indicating that it is in the metal's outer shell. In the NMR structure of human immunodeficiency virus type 1 (HIV-1) reverse transcriptase RNase H domain solved in 80 mM $MgCl_2$ (Figure 1b),[16] the metal position is uncertain, but the orientation of the D′ (D76) carboxylate suggests monodentate binding to Mg^{2+}. In the Mg^{2+}-bound X-ray structure of maloney murine leukemia virus (MMLV) RNase H (Figure 1c),[17] the D′ (D87) carboxylate oxygen atoms are 2.0 and 2.8 Å from Mg^{2+}. Since a monodentately bound carboxylate should have a metal-free oxygen >3.5 Å from Mg^{2+}, this indicates an equilibrium between monodentate and

Received: January 18, 2013
Published: April 11, 2013

dx.doi.org/10.1021/ja4006095 | J. Am. Chem. Soc. 2013, 135, 6541−6548

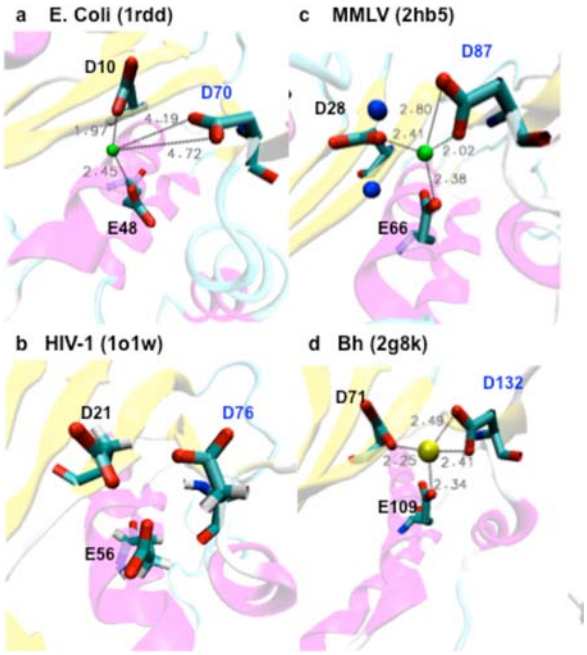

Figure 1. The Mg^{2+}-binding site in RNase H derived from (a) *E. coli* (1rdd), (b) HIV-1 (1o1w), (c) MMLV (2hb5), and (d) the Ca^{2+}-binding site in Bh RNase H (2g8k). The two blue spheres in MMLV RNase H are metal-bound water O atoms. Water molecules are not visible in other structures, while Mg^{2+} and bound water positions are not available in the 1o1w structure. The catalytically essential D′ in the DED′ motif is labeled in blue. The figures were generated using VMD.[56].

bidentate binding that is tilted in favor of monodentate binding. In the Ca^{2+}-bound X-ray structure of *Bacillus halodurans* (Bh) RNase H (Figure 1d),[18] the D′ (D132) carboxylate oxygen atoms are ∼2.4−2.5 Å from Ca^{2+}, indicating bidentate binding to Ca^{2+}. Although a fourth conserved carboxylate assists in the binding of a second metal ion,[18] our focus here is on the DED′ motif binding to the first metal ion.

The structures in Figure 1 indicate that the dication can bind to prokaryotic RNase H in different modes, defined by the number of metal-bound protein and water ligands. In aqueous solution, the first-shell coordination number (CN) of Mg^{2+} is 6,[19] whereas the CN of Ca^{2+} varies from 6 to 10, depending on the water to salt ratio and experimental conditions.[20] As illustrated in Figure 2, the first two carboxylates D and E of the DED′ motif bind monodentately to the metal dication by displacing two metal-bound water molecules; the third D′ carboxylate can bind the metal dication indirectly in the outer shell (referred to as outer-sphere complex) or directly via one (inner/outer-sphere complex) or both carboxylate oxygen atoms (inner-sphere complex). Comparison of the computed and experimental binding free energies of group IIA dications to *E. coli* RNase HI[10] suggests that Mg^{2+} prefers binding the first two carboxylates of the DED′ motif monodentately (Figure 2a), whereas Ca^{2+} prefers binding the third D′ carboxylate bidentately in addition to the Mg^{2+} ligands (Figure 2d). The additional interactions with both D′ carboxylate oxygen atoms enable Ca^{2+} to bind *E. coli* RNase HI tighter than Mg^{2+}, in accord with experimental observations.[8−10] When this essential D′ residue is bound to Ca^{2+}, it cannot serve as a proton/hydrogen-bond acceptor during the catalytic reaction and the net charge of the metal complex is −1 instead of 0; these changes may explain why Ca^{2+} binding to *E. coli* RNase HI abolishes enzymatic activity (see above).[10]

The X-ray/NMR structures and simulations together show that the native cofactor, Mg^{2+}, and the enzyme inhibitor, Ca^{2+}, can bind to the DED′ motif of RNase H enzymes in different, functionally nonequivalent modes that are characterized by the metal-binding mode of the catalytically essential D′. Since most studies focused on the interactions between Mg^{2+} or Ca^{2+} and first-shell ligands,[21−23] it is not clear if atoms outside the metal coordination sphere constituting the protein matrix have similar or different effects on the binding modes of Mg^{2+} vs Ca^{2+}. Thus, the free energy barriers for the binding of the catalytically essential D′ to Mg^{2+} and Ca^{2+} in *E. coli* RNase HI and MMLV RNase H have been computed using umbrella sampling and a classical force field (referred to as the "classical" model). They were compared with the corresponding barriers in water using the same simulation protocol and force field. By comparing the free energy barriers for the same binding process in different media (protein vs water), systematic errors in the computed barriers (e.g., from the classical force field) would largely cancel. Although the ion parameters had been developed to reproduce experimental solution data,[24] which implicitly take into account electronic effects of the metal cation, it is not clear the extent to which these parameters capture the different electronic effects of Mg^{2+} and Ca^{2+}.[23,25] Hence, the binding in water was also studied using density functional theory (DFT) and a self-consistent reaction field (SCRF) (referred to as the "QM" model) to elucidate the similarities and differences between the classical and quantum models. The results show that atoms remote from the metal-binding site as well as the enzymes's 3D architecture affect the binding kinetics of the catalytically essential D′ in RNase H enzymes to the native cofactor Mg^{2+} more than that to its competitor Ca^{2+}.

METHODS

Molecular Dynamics (MD) Simulations. (a) Protonation States. MD simulations using the program CHARMM34[26] were carried out on fully solvated metal-bound RNase HI at a mean temperature of 300 K and at physiological pH. All Asp/Glu were deprotonated, while all lysines and arginines were protonated. According to the measured His pK_a values in *E. coli* RNase HI,[27] the histidines were protonated except for H83 (pK_a = 5.5) and H114 (pK_a = 5.0), which were deprotonated at $N^{\delta 1}$. As the H83 and H114 imidazole rings are 25 and 22 Å, respectively, from Mg^{2+}, their protonation states are unlikely to affect the relative metal-binding affinity. Since the His pK_a values in MMLV RNase H have not been determined, the protonation states of the histidines were assigned according to the computed free energies for transferring a proton from $N^{\delta 1}$ to $N^{\epsilon 2}$ and adding a proton to $N^{\epsilon 2}$ of the imidazole side chain in the enzyme, as compared to explicit water. The relative free energies in Supporting Information Table S1 indicate that all the histidines are neutral with a proton at $N^{\delta 1}$ except H96, which is protonated at $N^{\epsilon 2}$ instead of $N^{\delta 1}$.

(b) Force Field. The MD simulations employed the all-hydrogen CHARMM22 force field for the protein atoms,[28] the TIP3P[29] water model, and periodic boundary conditions in a truncated octahedron primary box.[30] The ion−water interaction energies were modeled by a sum of Coulomb and van der Waals pairwise energies. The ion parameters were derived using the procedure outlined in our previous work[24] starting from modified Åqvist Mg^{2+} parameters,[31] which reproduced the absolute solvation free energy of Mg^{2+}. These parameters could reproduce the experimental ion−water distances, CNs, and relative hydration free energies (see Table 1). They were then used in conjunction with traditional combining rules for ion−protein interactions in the simulations. The classical force field was not reparameterized to account for the different electronic effects of Mg^{2+}

dx.doi.org/10.1021/ja4006095 | J. Am. Chem. Soc. 2013, 135, 6541−6548

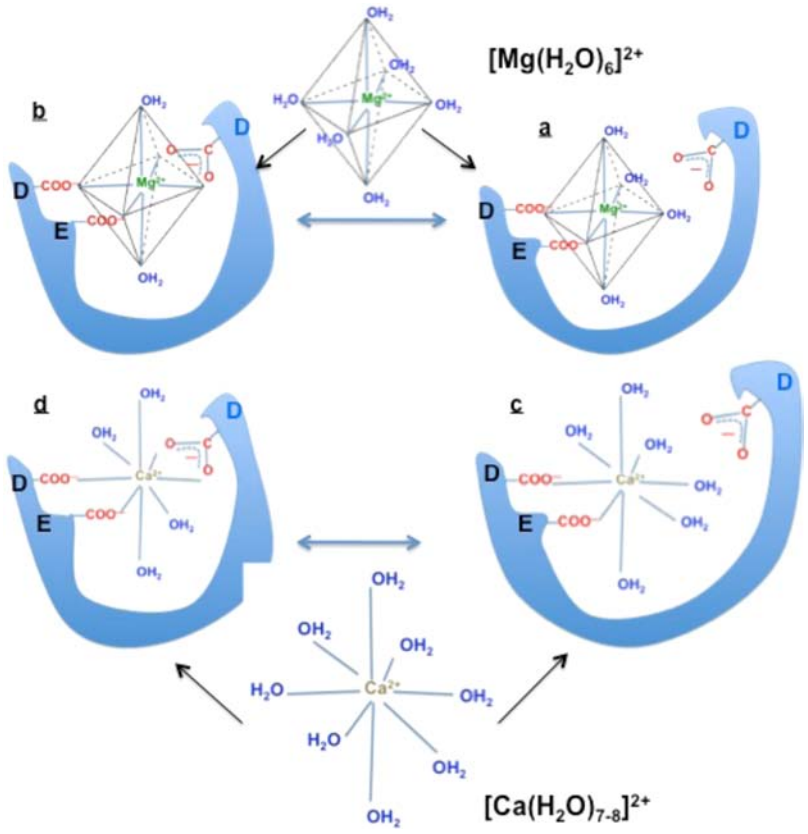

Figure 2. A schematic diagram for the binding of Mg^{2+} vs Ca^{2+} to the DED′ motif in the RNase H cavity. Mg^{2+}, which has a more favorable hydration free energy than Ca^{2+} by ∼75 kcal/mol, prefers to bind to the third carboxylate in the outer shell (a), whereas Ca^{2+} prefers to bind bidentately to the third carboxylate (d).

Table 1. Computed and Experimental Structural and Thermodynamics Properties of Divalent Cations in Water

ion	ε^a (kcal/mol)	$R_{min}/2^a$ (Å)	$R_{ion}{}^b$ (Å)	$R_{Born}{}^c$ (Å)	$R_{ion-O}{}^d$ (Å)	CN^e	$\Delta\Delta G_{solv}{}^f$ (kcal/mol)	$\Delta G_{solv}{}^{expt,g}$ (kcal/mol)
Mg^{2+}	0.6560	0.8758	0.72	1.44	2.03 ± 0.06 (2.09)	6 (6)	−75.6 ± 0.1 (−74.7)	−455.5
Ca^{2+}	0.0551	1.6252	1.00	1.72	2.45 ± 0.10 (2.42)	7.5 (7−8)	0.0	−380.8

[a]van der Waals parameters taken from Babu et al., 2003.[10] [b]Ionic radius for a CN of 6 from Shannon, 1976.[54] [c]Born radius computed from the experimental free energy in the last column; i.e., $R_{Born} = -655.5/\Delta G_{solv}{}^{expt}$. [d]Average ion−oxygen(water) distances computed from simulations; experimental values taken from Marcus, 1988[19] are in parentheses. [e]The computed ion−water CNs in the first solvation shell; experimental values taken from Marcus, 1988[19] are in parentheses. [f]The computed and experimental (in parentheses) hydration free energies relative to the hydration free energy of Ca^{2+}. [g]Experimental absolute hydration free energies from Friedman and Krishnan, 1973.[55]

and Ca^{2+}, as our key goal was to assess the differential effects of the protein matrix (relative to water) upon binding of a catalytic aspartate to Mg^{2+} vs Ca^{2+}.

All bonds involving hydrogen atoms were constrained during the simulations using the SHAKE algorithm.[32] The nonbonded interactions were truncated at 18 Å using a force-switching function in the region from 14 to 17 Å. They were also treated using the particle mesh Ewald algorithm[33] to verify that the relative free energy barriers are not very sensitive to long-range interactions.[34]

(c) Simulation Protocol. The starting structures for the simulations of *E. coli* RNase HI and MMLV RNase H are the respective Mg^{2+}-bound X-ray structures (PDB entries 1rdd and 2hb5). Hydrogen atoms were added to the crystal structures, and their positions were energy minimized. All the simulations employed the same truncated octahedron of cubic edge length 70 Å containing TIP3P water molecules. The solute orientation in the primary box was optimized to ensure sufficient solvation of all parts of the protein.[35] The simulation protocol described in our previous work[10] was used except for the longer nonbond cut-off used here. After 500 ps of equilibration, simulations of RNase H bound to Mg^{2+} or Ca^{2+} in different modes were performed for 1 ns; the root-mean-square deviation of the Mg-bound RNase H structures from the respective crystal structure is 1.3 to 1.5 Å.

Reaction Modeled and Reaction Coordinate. The reaction modeled is the binding of the D′ carboxylate of the DED′ motif to the metal ion (Mg^{2+} or Ca^{2+}). Since either or both D′ carboxylate oxygen atoms can bind the metal ion, we chose the mean of the two ion−oxygen distances (R_{c1} and R_{c2} in Figure 3) as the reaction coordinate; i.e., $R_c = (R_{c1} + R_{c2})/2$. Such an R_c choice has the advantage of simultaneously describing D′ binding in the outer, inner/outer, or inner-sphere carboxylate-binding mode. For a carboxylate monodentately bound to Mg^{2+} in water, the distance from Mg^{2+} to the bound carboxylate oxygen in the QM model is ∼2.12 Å, while that to the metal-free carboxylate oxygen is ∼3.65 Å; hence, $R_c = (2.12 + 3.65)/2 = 2.9$ Å. Likewise, the R_c corresponding to a carboxylate monodentately bound to Ca^{2+} in water is $(2.50 + 3.85)/2 = 3.18$ Å. For a bidentately bound carboxylate in water, the distance from the metal to either carboxylate oxygen is similar and R_c is ∼2.2 Å for Mg^{2+} and ∼2.5 Å for Ca^{2+}. On the other hand, for a D′ carboxylate bound in the outer sphere, the energy minimum in water occurs at an R_c of ∼5.0 Å for Mg^{2+} and ∼5.5 Å for Ca^{2+}. In summary, a binding mode with an energy minimum beyond 4 Å indicates an outer-sphere carboxylate, whereas that at R_c ∼3 Å indicates a monodentately bound, inner/

dx.doi.org/10.1021/ja4006095 | J. Am. Chem. Soc. 2013, 135, 6541−6548

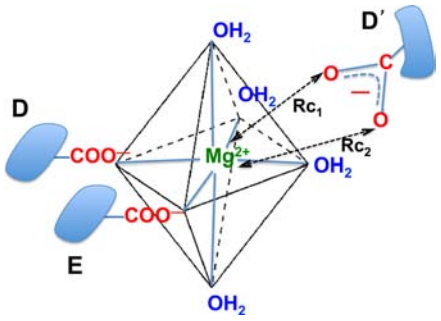

Figure 3. The reaction coordinate, R_c, is defined as $(R_{c1} + R_{c2})/2$. The incoming acidic residue D′ is D70 in *E. coli* RNase HI and D87 in MMLV RNase H.

outer-sphere carboxylate, while that at $R_c \leq 2.5$ Å indicates a bidentately bound, inner-sphere carboxylate.

Umbrella Sampling Calculations. (a) Free Energy Profiles in Protein. MD simulations were performed with umbrella potentials applied to the reaction coordinate of each window, which was placed every 0.2 Å from 5.2 Å to 2.3 Å (Mg^{2+}) or 2.6 Å (Ca^{2+}) with additional windows around the maxima/minima. As the reaction coordinate spans a narrow range of 2−4 Å, a biasing Morse potential with a force constant of 100 kcal/mol/Å^2 was needed to sample either side of the windows, as a force constant less than 100 kcal/mol/Å^2 cannot sample the very steep barrier owing to too large displacements.[36] At each window, the initial configuration, obtained from the previous window simulation, was independently re-equilibrated for 100 ps before a production run of 500 ps, which was used to generate population histograms. Since the windows were independently equilibrated, reverse sampling of the reaction coordinate was not performed. The weighted histogram analysis method (WHAM),[37,38] implemented in Grossfield's program,[39] was used to construct the free energy profile. The UMBRELLA module of the CHARMM34 program was used to compute the free energy barriers in each window.[26,40] When R_c is >4.6 Å and <2.2 Å (Mg^{2+}) or <2.6 Å (Ca^{2+}), 1 ns unbiased simulations were performed and the R_c and free energy well for the inner-sphere complex was joined with the WHAM free energy profile to obtain the full profile.

(b) Free Energy Profiles in Water. Similar umbrella sampling calculations were performed for ions interacting with isolated carboxylates in water. Their initial configurations were obtained from the respective simulations in protein solution with the Asp/Glu side chain modeled by acetate. As our goal was to determine how the free energy as a function of R_c (potential of mean force) in protein solution would differ from the corresponding potential of mean force in water, the atomic charges of acetate were kept identical to those of the Asp/Glu side chain; i.e., −0.76e for the carboxyl oxygen and 0.62e for the carboxyl carbon. The metal−carboxylate complex was centered in a truncated octahedral box of edge length 55 Å containing 2778 TIP3P water molecules after removing water molecules that overlapped with the heavy solute atoms. The water calculations employed the same simulation protocol and treatment of nonbonded interactions as the protein calculations. For the unbiased simulations with D′ in the metal's outer sphere, the free carboxylate may escape into the bulk solution owing to the strong solvation of its negative charge; hence, a slight force constant of 0.5 kcal/mol/Å^2 was used to restrict D′ in the vicinity of the metal ion. No correction term for this mild force constant was applied, as the simulation of the outer-sphere complex was used only to determine the relative position of the potential of mean force for the inner-sphere complex.

(c) Error Estimation of Free Energies. To estimate the statistical errors in the free energies, we used a boot-strap Monte Carlo error analysis, as implemented in Grossfield's program.[39] To establish convergence of the profiles, two more independent trajectories were generated at each window; the configurations were the same as the first set of simulations, but different sets of velocities were assigned to them and they were re-equilibrated. Thus, the free energies and corresponding error bars in protein/water were computed from an average of three trajectories.

DFT/SCRF Calculations. Energy Profiles in Water. To estimate electronic effects in the binding of Mg^{2+} vs Ca^{2+}, the energy profile of an outer-sphere acetate binding to Mg^{2+} or Ca^{2+} that was already bound to two acetates monodentately and solvated by 15 water molecules was computed using density functional theory (DFT) and a self-consistent reaction field (SCRF) solvent model. The reaction coordinate is the same as that used in the classical simulations, except that the approach of the carboxylate was symmetrical along the vector connecting the metal and carboxyl carbon; i.e., $R_{c1} = R_{c2}$ in Figure 3. Using the B3-LYP/6-31+G* method, the solvated metal complexes were constrained, optimized with R_c fixed, but fully optimized when the third carboxylate was in the outer sphere or bound to the metal. Since the basis set superposition error changed the energy difference between the fully optimized outer-sphere and inner-sphere Mg complexes by only 1.3 kcal/mol, it was not included in the DFT calculations.[41]

Bulk solvent effects were estimated using the SCRF method[42,43] by placing the solvated metal complex in a spherical cavity of radius 12 Å surrounded by a continuous medium with a dielectric constant of 80, and reoptimizing the structure. The choice of the cavity radius, which was determined from half the maximum distance between any two atoms including their van der Waals radii in the complex, did not significantly affect the energy. Bulk solvent effects were also estimated by solving the Poisson equation using the finite-difference method[44−46] for the fully optimized Mg^{2+} and Ca^{2+} complexes; the resulting free energies were similar to those obtained by the SCRF method to within 1 kcal/mol. All geometry optimizations were performed using the QChem 3.1 program,[47] followed by the Gaussian 09 program.[48]

RESULTS

Thermodynamic Stability of Mg^{2+} vs Ca^{2+}−Carboxylate Structures in Water. Binding of an acetate to a neutral $[Mg(H_2O)_4(CH_3COO)_2]^0$ or $[Ca(H_2O)_5(CH_3COO)_2]^0$ complex has been shown to be thermodynamically favorable in water.[22] To determine if a third carboxylate prefers to bind monodentately or bidentately to the metal, a third acetate was placed in the outer and inner coordination sphere of the solvated metal−dicarboxylate complexes. The resulting optimized structures show that, in water, a third carboxylate prefers to bind in the outer sphere to Mg^{2+}, but directly to Ca^{2+} via both its oxygen atoms. In the presence of three acetates in water, Mg^{2+} formed three stable octahedral complexes: (i) an *outer*-sphere complex where the oxygen atoms of the third carboxylate are >4.5 Å from Mg^{2+} (Figure 4a), (ii) an *inner/outer*-sphere complex where all three carboxylates are monodentately bound to Mg^{2+} (Figure 4b), and (iii) an *inner*-sphere complex where D′ is bidentately bound (Figure 4c). The stability of the three complexes decreased in the order outer-sphere > inner/outer-sphere > inner-sphere. Like Mg^{2+}, Ca^{2+} also formed three stable tricarboxylate complexes in water: (i) an *outer*-sphere complex where the oxygen atoms of the third carboxylate are >5.5 Å from Ca^{2+} (Figure 5a), (ii) an *inner/outer*-sphere complex where all three carboxylates are monodentately bound to Ca^{2+} (Figure 5b), and (iii) an *inner*-sphere complex with the third carboxylate bidentately bound to Ca^{2+} (Figure 5c). Unlike Mg^{2+}, the stability of these complexes decreased in the order inner-sphere > outer-sphere > inner/outer-sphere.

Kinetic Stability of Mg^{2+} vs Ca^{2+}−Carboxylate Structures in Water. To determine the kinetic barrier for binding of an outer-shell acetate in Figure 4a to Mg^{2+} in water, the binding energy was computed as a function of the reaction coordinate R_c (where $R_{c1} = R_{c2}$ in Figure 3) using DFT and an

dx.doi.org/10.1021/ja4006095 | J. Am. Chem. Soc. 2013, 135, 6541−6548

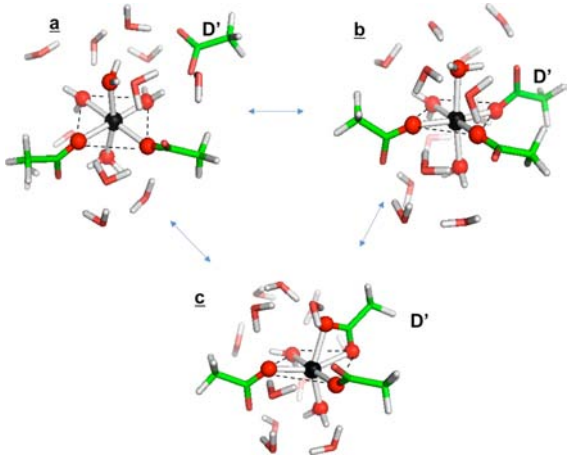

Figure 4. Fully optimized structures of solvated Mg^{2+} bound to two acetates monodentately and a third acetate in (a) the outer coordination sphere, (b) the inner/outer sphere, and (c) the inner sphere at the B3LYP/6-31+G* level. The R_c for D′ is 4.65 Å for (a), 2.8 Å for (b), and 2.2 Å for (c). The 4-fold octahedral plane is indicated by the dashed line.

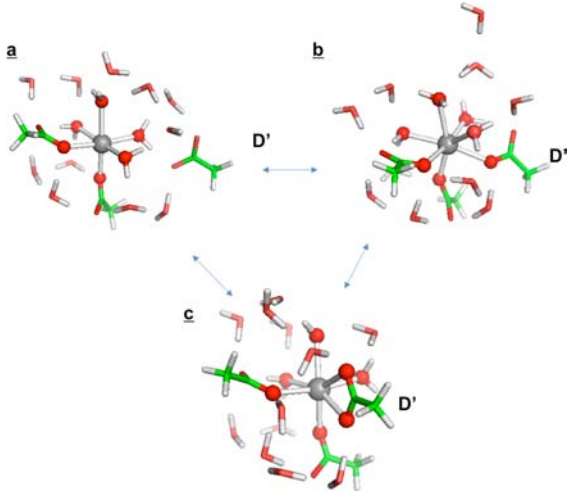

Figure 5. Fully optimized structures of solvated Ca^{2+} bound to two acetates monodentately and a third acetate in (a) the outer coordination sphere, (b) the inner/outer sphere, and (c) the inner sphere at the B3LYP/6-31+G* level. The R_c for D′ is 4.9 Å for (a), 3.2 Å for (b), and 2.5 Å for (c).

SCRF (QM model). The resulting energy profile in Figure 6 (black curve) predicts a high kinetic barrier (~18 kcal/mol) for binding of an outer-shell carboxylate to Mg^{2+} that is already monodentately bound to two carboxylates in water. A similar barrier (~20 kcal/mol) was obtained using a different reaction coordinate defined as the distance between the metal ion and the carboxylate carbon. The broad energy well between 5−5.5 Å in Figure 6 corresponds to a carboxylate in the outer coordination sphere (outer-sphere complex). As R_c decreased, the energy gradually increased and peaked at R_c ~3.1 Å. A local minimum appeared at R_c ~2.8 Å, corresponding to three carboxylates monodentately bound to Mg^{2+} (inner/outer-sphere complex). Another deep minimum was found at R_c ~2.2 Å, where the incoming carboxylate was bidentately bound to Mg^{2+} (inner-sphere complex).

To evaluate how the binding of an outer-shell carboxylate to Ca^{2+} in water would differ from that to Mg^{2+}, the corresponding

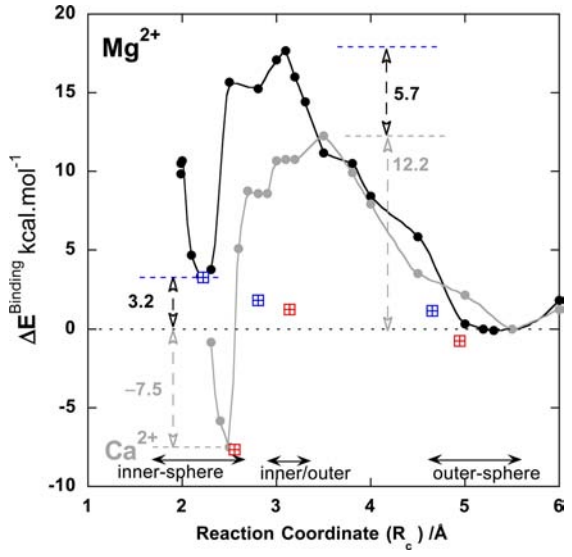

Figure 6. QM binding energy of an outer-sphere acetate to solvated Mg^{2+} (black curve) or Ca^{2+} (gray curve) that is already bound to two acetates in water as a function of the reaction coordinate, R_c, where $R_{c1} = R_{c2}$. The free energies of the constrained optimized structures for a fixed R_c were computed using DFT and a SCRF solvation model. The squares indicate the free energies of the unconstrained (free R_c) optimized structures of solvated Mg^{2+} (blue) and Ca^{2+} (red) bound to the third acetate in the inner, inner/outer, and outer-sphere modes.

energy profile for binding of an outer-shell acetate in Figure 5a to Ca^{2+} in water was computed using the QM model. Comparison of the binding energy profiles in Figure 6 for Mg^{2+} (black curve) and Ca^{2+} (gray curve) shows that it is easier for an outer-sphere carboxylate to bind directly to Ca^{2+} than to Mg^{2+} in water: The energy barrier for an outer-shell acetate to bind monodentately to Ca^{2+} is smaller than that to Mg^{2+} (by 5.7 kcal/mol). These findings reflect the ease of removing inner-shell water molecules from Ca^{2+} compared to Mg^{2+}, as evidenced by the longer metal−O(water) distance and smaller hydration free energy for Ca^{2+} compared to those for Mg^{2+} (Table 1). Relative to the outer-sphere complex, the inner-sphere complex is more stable (by 7.5 kcal/mol) for Ca^{2+}, but it is less stable (by 3.2 kcal/mol) for Mg^{2+}.

QM vs Classical Models. Since the free energy barriers for the binding of D′ to Mg^{2+} and Ca^{2+} in the RNase H enzymes were computed using classical force field models with umbrella sampling MD simulations (referred to as the "classical model"), it is important to first assess the reliability of the classical force field employed. Although the ion parameters in the classical force field were developed to reproduce experimental data (ion solvation free energies and ion−water CN and distances; see Table 1),[24] it is not clear if they can account for the different electronic properties of Mg^{2+} and Ca^{2+}. Thus, we computed the free energy for binding of an outer-shell acetate to Mg^{2+} and Ca^{2+} as a function of R_c in water using the classical model (Figure 7). However, the absolute free energy cannot be directly compared to the corresponding QM quantity, which neglected thermal sampling of the solute conformations and solute entropy. In computing the free energy *difference* for the same reaction involving different metal ions, the entropic changes for the Mg^{2+} and Ca^{2+} complexes would partly cancel. Hence, the "classical" free energy difference between the Mg^{2+} and Ca^{2+} complexes was compared to the corresponding QM energy difference.

dx.doi.org/10.1021/ja4006095 | J. Am. Chem. Soc. 2013, 135, 6541−6548

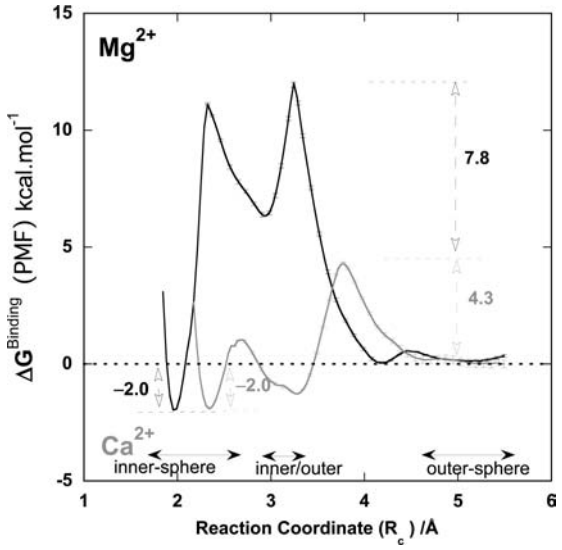

Figure 7. Potential of mean force (free energy profiles) for the binding of an outer-sphere acetate to Mg^{2+} (black curve) or Ca^{2+} (gray curve) already bound to two acetates in water as a function of the reaction coordinate, R_c, in Figure 3. The free energies were computed from umbrella sampling MD simulations using a classical force field, and the error bars were obtained from three independent trajectories (see Methods).

The classical model could capture key features of the rate-limiting step; viz., monodentate binding of an outer-shell acetate to the metal ion: Both QM and classical models predicted a smaller barrier for an outer-sphere carboxylate to bind monodentately to Ca^{2+} than to Mg^{2+} in water. Whereas the QM model predicted the *inner*-sphere Mg^{2+} complex to be *less* stable (by ∼3 kcal/mol) but the *inner*-sphere Ca^{2+} complex to be more stable than the respective outer-sphere complex, the classical model predicted both *inner*-sphere Mg^{2+} and Ca^{2+} complexes to be equally more stable than their outer-sphere complexes (by ∼2 kcal/mol). These differences could be attributed to the differential charge transfer effects of the two metal ions that are absent in the classical model: In the QM model, Mg^{2+}, being a stronger Lewis acid than Ca^{2+}, can accept more charge from the three metal-bound acetates than Ca^{2+}; since the positive charge on Mg^{2+} is less than that on Ca^{2+} in the inner/outer-sphere complex, Mg^{2+} cannot compete for the free carboxylate oxygen as well as Ca^{2+} can. On the other hand, the classical model does *not* take into account the significant charge transfer from the three negatively charged carboxylates to the metal cation or the different charge-accepting abilities of the two metal cations; Mg^{2+} and Ca^{2+} have the same high charge of +2e and can both bind the third carboxylate bidentately equally well.

Effects of Protein Matrix on Mg^{2+} vs Ca^{2+} Binding. Since Figures 6 and 7 show that the first water→carboxylate exchange is rate limiting, the free energy barriers for the catalytically essential D′ of the DED′ motif in *E. coli* RNase HI and MMLV RNase H domain to bind monodentately to Mg^{2+} and Ca^{2+} were computed. The free energy barriers do not seem to be sensitive to long-range electrostatic interactions, as the barriers computed using the particle mesh Ewald algorithm (Figure 8, dashed green curve) are similar to those computed using an 18 Å cutoff (Figure 8, solid green curve).[36] Similar effects on the ion−ion potential of mean forces were reported in previous works.[34] To elucidate the role of the protein matrix,

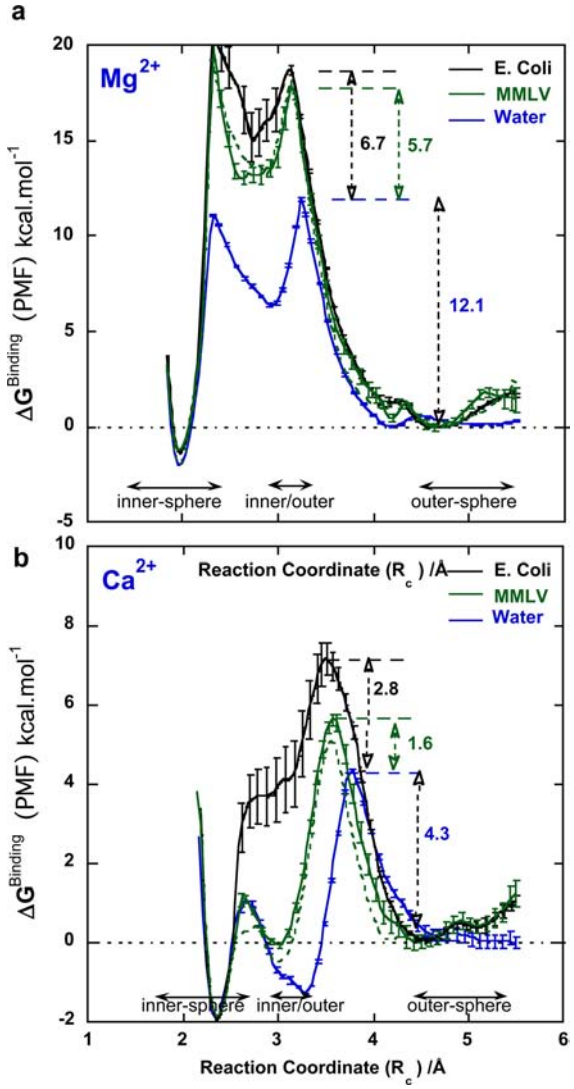

Figure 8. Comparison of the potential of mean force (free energy profiles) for the binding of an outer-shell carboxylate to (a) Mg^{2+} and (b) Ca^{2+} bound in a carboxylate cavity in water (blue curve), in *E. coli* RNase HI (black curve) and in MMLV RNase H (green curve, with dashed curve for PME method). The vertical bars at selected points indicate error bars obtained from three trajectories (see Methods).

the free energy barriers in the enzyme (Figure 8, black and green curves) were compared to those in water (Figure 8, blue curve).

The results in Figure 8 and Table 2 reveal the differential role of the protein matrix upon binding of D′ to Mg^{2+} vs Ca^{2+}. The protein matrix affects binding of the catalytically essential D′ to the native Mg^{2+} cofactor more than the respective binding to the enzyme inhibitor, Ca^{2+}: The free energy barrier for D′ to bind monodentately to Mg^{2+} in both *E. coli* and MMLV enzymes is significantly larger than that in water (by 5.7 to 6.7 kcal/mol), whereas that to Ca^{2+} in protein solution is only slightly higher than that in water (by 1.6 to 2.8 kcal/mol). Thus, the enzyme and its aqueous environment collectively make it much harder for a third carboxylate D′ to bind directly to Mg^{2+} than to Ca^{2+}: The free energy barrier difference between an outer-shell carboxylate binding to Mg^{2+} and Ca^{2+} in *E. coli* (18.8 − 7.1 = 11.7 kcal/mol) or MMLV (17.8 − 5.9 = 11.9 kcal/mol) RNase H is larger than the corresponding difference in water (12.1 − 4.3 = 7.8 kcal/mol) by ∼4 kcal/mol.

dx.doi.org/10.1021/ja4006095 | J. Am. Chem. Soc. 2013, 135, 6541−6548

Table 2. Free Energy Barriers As a Function of the Reaction Coordinate R_c for an Outer-Shell Carboxylate to Bind Monodentately to Mg^{2+} in Water, *E. coli* RNase H, and MMLV RNase H

ion	R_c (Å)	$\Delta\Delta G_{sln}{}^{a,b}$ (kcal/mol)	enzyme	R_c (Å)	$\Delta\Delta G_{enz}{}^{c,b}$ (kcal/mol)	$\Delta\Delta G_{enz} - \Delta\Delta G_{sln}$ (kcal/mol)
Mg^{2+}	3.25	12.06 ± 0.11	*E. coli*	3.12	18.75 ± 0.30	6.69
			MMLV	3.14	17.80 ± 0.60	5.74
Ca^{2+}	3.78	4.30 ± 0.04	*E. coli*	3.53	7.11 ± 0.41	2.81
			MMLV	3.59	5.90 ± 0.14	1.60

[a]Free energy barrier computed in pure water (see Methods). [b]The barrier is relative to the minimum corresponding to the outer-sphere complex; the error bars were obtained from three independent simulations and a Monte Carlo boot-strap analysis implemented in the WHAM program.[39] [c]Free energy barrier in the enzyme cavity.

To elucidate the differential binding of a third carboxylate to Mg^{2+} and Ca^{2+} in *E. coli* RNase H1, the M−O^{water} CNs, M−O distances, and O−M−O angles (where M = Mg^{2+} or Ca^{2+}) were computed from the MD simulations of the outer-sphere and outer/inner-sphere metal complexes in *E. coli* RNase H1. The results in Figure S1 and Table S2 suggest that as the outer-shell D′ carboxylate approaches the metal ion, it is more difficult for the RNase H matrix to maintain the rigid and strict coordination geometry requirements of Mg^{2+} compared to the larger Ca^{2+}. For both the outer-sphere and outer/inner-sphere complexes in *E. coli* RNase H1, Mg^{2+} formed a rigid, octahedral complex with an average O−Mg−O angle of 90° and standard devation of ≤0.4°; in contrast, Ca^{2+} is seven-coordinated and its coordination shell is much more flexible with an average O−Ca−O angle of 54° and a standard deviation ranging from 10° to 12° (Table S2).

CONCLUDING DISCUSSION

Role of the Protein Matrix. An interesting finding herein is that the protein matrix affects metal binding to the RNase H active site, but the magnitude of the effects depends on the metal ion. Compared to water, the protein matrix hinders binding of a third carboxylate to water (see Table 2, last column), probably because it is harder for the protein dipoles to readjust to the incoming carboxylate than the water dipoles. Furthermore, the protein matrix hinders binding of the catalytically essential D′ to the native Mg^{2+} cofactor much more than the respective binding to the enzyme inhibitor, Ca^{2+}. This may be partly due to the differences in coordination preference and flexibility of the two metal ions, as found in the MD simulations of the outer-sphere and outer/inner-sphere complexes in *E. coli* RNase H1 (see Figure S1 and Table S2). This is consistent with the empirical finding that Mg^{2+} strongly prefers the octahedral coordination geometry, whereas Ca^{2+} can adopt various coordination geometries with CNs ranging from 6 to 8 in metal complexes.[49] Thus, it seems to be easier for the RNase H protein matrix to maintain the flexible coordination geometry of Ca^{2+}, as compared to Mg^{2+}.

Biological Implications. The Mg-bound RNase H crystal structures indicate that D′ can bind the native Mg^{2+} cofactor in the outer-sphere (Figure 1a) or an inner/outer-sphere mode (Figure 1c). The binding mode observed in the Mg-bound RNase H crystal structures probably depends on the crystallization conditions and process. While the high free energy barrier for D′ to bind monodentately to Mg^{2+} could be overcome during the crystallization process, it could temporarily trap D′ in the metal's outer sphere during enzyme preorganization. This would leave the catalytically essential D′ free to serve as a proton/hydrogen-bond acceptor, while maintaining the neutrality of the metal complex; furthermore, the water-rich Mg^{2+} is a source of confined water molecules for hydrogen-bonding interactions or activation/generation of a nucleophile[50,51] for the catalytic reaction when the substrate is bound.[7,51] At high metal ion concentrations, a second Mg^{2+} could bind to RNase H either before or together with the substrate. It would be interesting for future studies to evaluate how the free energy profiles (Figure 8) change upon binding a second metal cation and/or substrate.

Physical Basis for the Different Metal-Binding Modes in Water. This work has also revealed the different preferred Mg^{2+} and Ca^{2+} carboxylate-binding modes in water as well as the physical basis for this difference. In water, Ca^{2+} prefers to bind one of the three carboxylates bidentately, in contrast to Mg^{2+} (see Figure 6). This difference in the carboxylate-binding modes found for Mg^{2+} and Ca^{2+} in water is due to the significant charge transfer from the three carboxylates as well as the different charge-accepting ability and CN preference of the two metal dications. As Ca^{2+} is a poorer charge acceptor than the smaller Mg^{2+}, a charge transfer from the three monodentately bound acetates reduced the positive charge on Ca^{2+} less than that on Mg^{2+}. Hence, Ca^{2+} could apparently outcompete the neighboring water hydrogen for the free oxygen of the third carboxylate.[21,52] Furthermore, the larger CN of Ca^{2+} compared to that of Mg^{2+} would enhance steric repulsion among the ligands, so the relative size of the ligand becomes important. A bidentately bound carboxylate is less space-demanding than its competing counterpart; i.e., a monodentately bound carboxylate hydrogen-bonded to a water: The distance between the two O atoms of a bidentately bound carboxylate is 2.2 Å in Figure 5c, whereas the distance between a monodentately bound carboxylate O and the nearest metal-bound water O is 3.1 Å in Figure 5b. Hence, the metal-free O of the third carboxylate preferred to bind directly to Ca^{2+} in water.

Limitations of Classical Simulations. The above results help to pinpoint the rather subtle differences between classical and quantum models. The classical model could not capture the *thermodynamic* differences between Mg^{2+} and Ca^{2+} binding to a third carboxylate in water: It predicted that a third carboxylate would bind bidentately to Mg^{2+} to form an inner-sphere complex that is more stable than the corresponding outer-sphere one, in contrast to the QM model. This is because the classical force field does not take into account charge transfer and polarization effects[53] as well as the different charge-accepting ability of Mg^{2+} vs Ca^{2+} (see above). On the other hand, the classical model could capture the *kinetic* differences between Mg^{2+} and Ca^{2+} binding to an outer-shell carboxylate in water, especially for the first water→carboxylate exchange: It yielded a free energy barrier for Mg^{2+} relative to that for Ca^{2+} (7.8 kcal/mol, Figure 7), which is comparable to that obtained from the QM model (5.7 kcal/mol, Figure 6). The higher barrier for Mg^{2+} compared to Ca^{2+} in water reflects the greater

dx.doi.org/10.1021/ja4006095 | J. Am. Chem. Soc. 2013, 135, 6541−6548

dehydration penalty for Mg^{2+} vs Ca^{2+}, which is accounted for in the classical force field employed since the parameters have been developed to reproduce the experimental ion−water distances, CNs, and relative hydration free energies (see Table 1).

■ ASSOCIATED CONTENT

Supporting Information

Complete refs 28, 47, and 48; Figure S1 (pair distribution functions and corresponding running metal−O^{water} CNs); Table S1 (protonation states of histidines in MMLV RNase H); Table S2 (mean metal−O and O−metal−O angles in *E. coli* RNase H1); and Table S3 (coordinates of the optimized structures in Figures 4 and 5). This material is available free of charge via the Internet at http://pubs.acs.org.

■ AUTHOR INFORMATION

Corresponding Author

babu@ibms.sinica.edu.tw; carmay@gate.sinica.edu.tw

Notes

The authors declare no competing financial interests.

■ ACKNOWLEDGMENTS

This work was supported by the National Science Council, Taiwan, NSC Contract No. NSC 98-2113-M-001-011-MY5 and Academia Sinica.

■ REFERENCES

(1) Sigel, H. *Metal Ions in Biological Systems*; Marcel Dekker: New York, 1974.
(2) Cowan, J. A. *Biological Chemistry of Magnesium*; VCH: New York, 1995.
(3) Nicholson, A. W. *Ribonucleases: Structures and Functions*; Academic Press: 1997.
(4) Cowan, J. A. *Chem. Rev.* **1998**, *98*, 1067.
(5) Bertini, I., Sigel, A., Sigel, H., Eds. *Handbook on Metalloproteins*; Marcel Dekker: New York, 2001.
(6) *Nucleases*; Hostomsky, Z., Hostomska, Z., Matthews, D. A., Eds.; Cold Spring Harbor Laboratory: Cold Spring Harbor, NY, 1994.
(7) Yang, W.; Lee, J. Y.; Nowotny, M. *Mol. Cell* **2006**, *22*, 5.
(8) Black, C. B.; Cowan, J. A. *Inorg. Chem.* **1994**, *33*, 5805.
(9) Casareno, R., L. B.; Li, D.; Cowan, J. A. *J. Am. Chem. Soc.* **1995**, *117*, 11011.
(10) Babu, C. S.; Dudev, T.; Casareno, R.; Cowan, J. A.; Lim, C. *J. Am. Chem. Soc.* **2003**, *125*, 9318.
(11) Yang, W.; Steitz, T. A. *Structure* **1995**, *3*, 131.
(12) Venclovas, C.; Siksnys, V. *Nat. Struct. Biol.* **1995**, *2*, 838.
(13) Casareno, R. L. B.; Cowan, J. A. *Chem. Commun.* **1996**, 1813.
(14) Kanaya, S.; Kohara, A.; Miura, Y.; Sekiguchi, A.; Iwai, S.; Inoue, H.; Ohtsuka, E.; Ikehara, M. *J. Biol. Chem.* **1990**, *265*, 4615.
(15) Katayanagi, K.; Ishikawa, M.; Morikawa, K. *Proteins: Struct., Funct., Genet.* **1993**, *17*, 337.
(16) Pari, K.; Mueller, G. A.; DeRose, E. F.; Kirby, T. W.; London, R. E. *Biochemistry* **2003**, *42*, 639.
(17) Lim, D.; Gregorio, G.; Bingman, C.; Martinez-Hackert, E.; Hendrickson, W. A.; Goff, S. P. *J. Virol.* **2006**, *80*, 8379.
(18) Nowotny, M.; Yang, W. *EMBO J.* **2006**, *25*, 1924.
(19) Marcus, Y. *Chem. Rev.* **1988**, *88*, 1475.
(20) Ohtaki, H.; Radnai, T. *Chem. Rev.* **1993**, *93*, 1157.
(21) Dudev, T.; Lim, C. *J. Phys. Chem. B* **2004**, *108*, 4546.
(22) Dudev, T.; Lim, C. *J. Am. Chem. Soc.* **2006**, *128*, 1553.
(23) Dudev, T.; Lim, C. *Annu. Rev. Biophys.* **2008**, *37*, 97.
(24) Babu, C. S.; Lim, C. *J. Phys. Chem. A* **2006**, *110*, 691.
(25) Dudev, T.; Chang, L.-Y.; Lim, C. *J. Am. Chem. Soc.* **2005**, *127*, 4091.
(26) Brooks, B. R.; Bruccoleri, R. E.; Olafson, B. D.; States, D. J.; Swaminathan, S.; Karplus, M. *J. Comput. Chem.* **1983**, *4*, 187.
(27) Oda, Y.; Yoshida, M.; Kanaya, S. *J. Biol. Chem.* **1993**, *268*, 88.
(28) MacKerell, J. A. D.; et al. *J. Phys. Chem. B* **1998**, *102*, 3586.
(29) Jorgensen, W. L.; Chandrasekhar, J.; Madura, J. D.; Impey, R. W.; Klein, M. L. *J. Chem. Phys.* **1983**, *79*, 926.
(30) Allen, M. P.; Tildesley, D. J. *Computer Simulation of Liquids*; Oxford University Press: New York, 1987.
(31) Åqvist, J. *J. Phys. Chem.* **1990**, *94*, 8021.
(32) Ryckaert, J. P.; Ciccotti, G.; Berendsen, H. J. C. *J. Comput. Phys.* **1977**, *23*, 327.
(33) Darden, T.; York, D.; Pedersen, L. *J. Chem. Phys.* **1993**, *98*, 10089.
(34) Maksimiak, K.; Rodziewicz-Motowidlo, S.; Czaplewski, C.; Liwo, A.; Scheraga, H. A. *J. Phys. Chem. B* **2003**, *107*, 13496.
(35) Mezei, M. *J. Comput. Chem.* **1997**, *18*, 812.
(36) Babu, C. S.; Lim, C. *J. Am. Chem. Soc.* **2010**, *132*, 6290.
(37) Kumar, S.; Rosenberg, J. M.; Bouzida, D.; Swendsen, R. H.; Kollman, P. A. *J. Comput. Chem.* **1992**, *13*, 1011.
(38) Boczko, E. M.; Brooks, C. L., III. *J. Phys. Chem.* **1993**, *97*, 4509.
(39) Grossfield, A. *WHAM: the weighted histogram analysis method*, version 2.0.6; http://membrane.urmc.rochester.edu/content/wham.
(40) Kottalam, J.; Case, D. A. *J. Am. Chem. Soc.* **1988**, *110*, 7690.
(41) Yang, T.-Y.; Dudev, T.; Lim, C. *J. Am. Chem. Soc.* **2008**, *130*, 3844.
(42) Onsager, L. *J. Am. Chem. Soc.* **1936**, *58*, 1486.
(43) Kirkwood, J. G. *J. Chem. Phys.* **1939**, *7*, 911.
(44) Gilson, M. K.; Honig, B. H. *J. Comput. Chem.* **1988**, *9*, 327.
(45) Lim, C.; Bashford, D.; Karplus, M. *J. Phys. Chem.* **1991**, *95*, 5610.
(46) Bashford, D. In *Scientific Computing in Object-Oriented Parallel Environments*; Ishikawa, Y., Oldehoeft, R. R., Reynders, V. W., Tholburn, M., Eds.; Springer: Berlin, 1997; Vol. *1343*, p 233.
(47) Shao, Y.; et al. *Phys. Chem. Chem. Phys.* **2006**, *8*, 3172.
(48) Frisch, M. J. et al. *Gaussian 09*, revision A.02; Gaussian, Inc.: Wallingford, CT, 2009.
(49) Kuppuraj, G.; Dudev, M.; Lim, C. *J. Phys. Chem. B* **2009**, *113*, 2952.
(50) Rosta, E.; Nowotny, M.; Yang, W.; Hummer, G. *J. Am. Chem. Soc.* **2011**, *133*, 8934.
(51) De Vivo, M.; Dal Peraro, M.; Klein, M. L. *J. Am. Chem. Soc.* **2008**, *130*, 10955.
(52) Dudev, T.; Lim, C. *Acc. Chem. Res.* **2007**, *40*, 85−93.
(53) Sakharov, D.; Lim, C. *J. Am. Chem. Soc.* **2005**, *127*, 4923.
(54) Shannon, R. D. *Acta Crystallogr., Sect. A* **1976**, *32*, 751.
(55) Friedman, H. L.; Krishnan, C. V. In *Water: A Comprehensive Treatise*; Franks, F., Ed.; Plenum Press: New York, 1973; Vol. *3*, p 1.
(56) Humphrey, W.; Dalke, A.; Schulten, K. *J. Mol. Graphics* **1996**, *14*, 33.